Research Article | Open Access

Microstructures

Kang et al. Microstructures 2026, 6, 2026096 DOI:10.20517/microstructures.2026.76

Sintering aids engineering for high-performance energy storage in tungsten bronze ceramics

Ruirui Kang[1], Haichao Hu[1], Junbo Xu[1], Bian Yang[2], Yingying Zhao[3], Yangfei Gao[1], Jinyou Shao[1,4], Xiaojie Lou[1]

Keywords:
Dielectric capacitor, ferroelectrics, energy storage, tungsten bronze, relaxor ferroelectric

Citation: Kang, R.; Hu, H.; Xu, J.; Yang, B.; Zhao, Y.; Gao, Y.; Shao, J.; Lou, X. Sintering aids engineering for high-performance energy storage in tungsten bronze ceramics. *Microstructures* **2026**, *6*, 2026096. https://dx.doi.org/10.20517/microstructures.2026.76

Received: 21 Apr 2026
First Decision: 15 May 2026
Revised: 5 Jun 2026
Accepted: 25 Jun 2026
Published: 13 Jul 2026

Academic Editor:
Jungho Ryu
Copy Editor:
Ping Zhang
Production Editor:
Ping Zhang

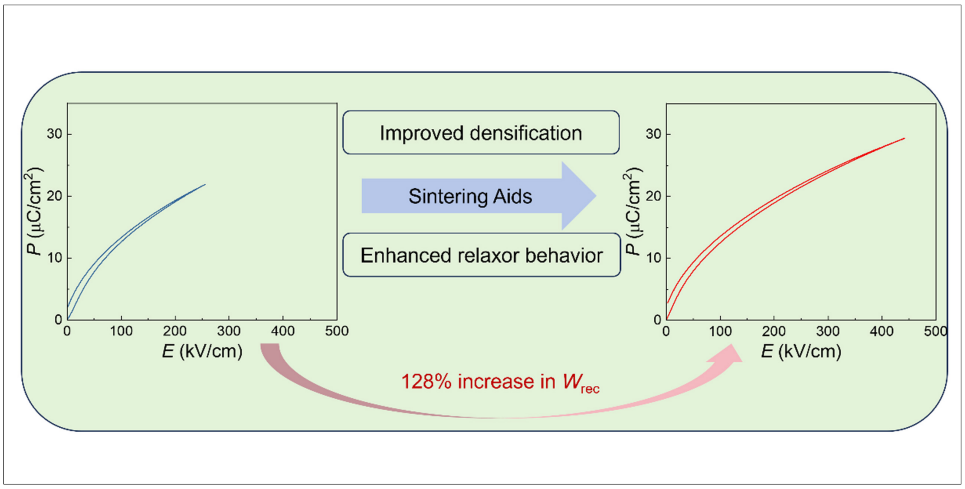

Abstract

Dielectric ceramics are critical for pulsed power applications owing to their high-power density and rapid charge-discharge capabilities. Among them, tetragonal tungsten bronze (TTB)-type ceramics have attracted attention as potential energy-storage materials due to their non-volatile compositions and structural adaptability. However, previous studies have primarily focused on regulating energy storage performance through multi-element doping, with relatively little attention paid to optimizing the sintering process to enhance the inherent performance of ceramics. In this work, we demonstrate an alternative and effective strategy to improve the intrinsic energy-storage performance in TTB-structured $Sr_{0.6}Ba_{0.4}Nb_2O_6$ (SBN) ceramics through the incorporation of sintering aids, including MnO_2, CuO, and Li_2CO_3, rather than complex compositional doping. The influence of these additives on the microstructure, dielectric behavior, and energy-storage characteristics is systematically investigated. Results show that CuO-modified SBN ceramics achieve a high

[1]Frontier Institute of Science and Technology, State Key Laboratory for Mechanical Behavior of Materials, Interdisciplinary Research Center of Frontier Science and Technology, Xi'an Jiaotong University, Xi'an 710049, Shaanxi, China.
[2]School of Materials Science and Engineering, Xi'an University of Technology, Xi'an 710048, Shaanxi, China.
[3]College of Materials Science and Engineering, Xi'an University of Science and Technology, Xi'an 710054, Shaanxi, China.
[4]Micro- and Nano-Technology Research Center, State Key Laboratory for Manufacturing Systems Engineering, Xi'an Jiaotong University, Xi'an 710049, Shaanxi, China.

Correspondence to: Dr. Ruirui Kang, Dr. Yangfei Gao, Prof. Jinyou Shao, Prof. Xiaojie Lou, Frontier Institute of Science and Technology, State Key Laboratory for Mechanical Behavior of Materials, Interdisciplinary Research Center of Frontier Science and Technology, Xi'an Jiaotong University, Xi'an 710049, Shaanxi, China. E-mail: krr0121@xjtu.edu.cn; gaoyangfei@xjtu.edu.cn; jyshao@xjtu.edu.cn; xlou03@xjtu.edu.cn

recoverable energy density of 4.41 J/cm³, representing a 128% enhancement compared to pristine SBN ceramic, along with an efficiency of 93.4%. This superior performance is attributed to the synergistic effects of enhanced densification and strengthened relaxor characteristics. Moreover, the ceramic presents excellent thermal (25-125 °C) and frequency stability (1-200 Hz). Our findings highlight sintering-aid engineering as a facile route to significantly enhance the energy-storage performance of SBN ceramics, thereby laying a foundation for the performance optimization of TTB-structured energy-storage ceramics.

INTRODUCTION

Dielectric ceramics are critical components in advanced pulse-power systems, benefiting from their high power density, rapid charge-discharge capability, and excellent reliability[1,2]. However, their energy storage density and efficiency still require substantial improvement to meet the growing demands of device miniaturization. The key figures of merit for energy storage, including total energy density (W_t), recoverable energy density (W_{rec}), and efficiency (η), are expressed as follows[3-5],

$$W_t = \int_0^{P_m} E dP \tag{1}$$

$$W_{rec} = -\int_{P_m}^{P_r} E dP \tag{2}$$

$$\eta = \frac{W_{rec}}{W_t} \times 100\% \tag{3}$$

where P_m and P_r denote the maximum and remnant polarization, respectively, and E represents the applied electric field. Therefore, to achieve high W_{rec} and η, it is essential to maximize ΔP (P_m - P_r) and enhance the breakdown electric field (E_b).

Dielectric materials are commonly classified into linear dielectrics, ferroelectrics, relaxor ferroelectrics, and antiferroelectrics[6]. Linear dielectrics exhibit low ΔP due to the absence of switchable dipoles[7-9]. Conventional ferroelectrics typically suffer from inferior energy storage performance because their microdomains lead to early polarization saturation under low electric fields[10], resulting in high P_r and low E_b. In contrast, relaxor ferroelectrics have attracted considerable interest for energy storage applications owing to their prominent ΔP and superior E_b[4,11,12]. These advantages stem from their characteristic nanodomain structure, which responds more quickly to external electric fields compared to the microdomains in normal ferroelectrics, thereby enabling higher W_{rec} and η.

In the past decade, research on relaxor ferroelectrics for energy storage applications has largely focused on perovskite-structured systems, such as $Bi_{0.5}Na_{0.5}TiO_3$[13,14], $BaTiO_3$[15,16], and $K_{0.5}Na_{0.5}Nb_{0.5}$[17,18] ceramics. Recently, tetragonal tungsten bronze (TTB)-structured dielectric ceramics, with the general chemical formula $(A1)_2(A2)_4C_4(B1)_2(B2)_8O_{30}$, have emerged as promising candidates for energy storage due to their structural versatility[19-21]. TTB compounds can be classified into three structural subtypes according to cation occupancy at the interstitial sites: the fully filled type (all A1, A2, and C sites occupied), the filled type (A1 and A2 fully occupied, C vacant), and the unfilled type (A1 and A2 partially occupied, C vacant). Among them, strontium barium niobate ($Sr_xBa_{1-x}Nb_2O_6$), an example of an unfilled tungsten bronze structure, has attracted much attention in the field of dielectric energy storage materials due to its non-volatile compositions and tunable relaxor behavior[22].

Recent advances in $Sr_xBa_{1-x}Nb_2O_6$-based ceramics have mainly relied on multi-element doping to tailor relaxor properties. For instance, Tang *et al.* achieved W_{rec} of 5.22 J/cm³ and an η of 83.4% in $Sr_{0.475}Ba_{0.475}La_{0.1}Hf_{0.1}Ti_{0.1}Sb_{0.2}Ta_{0.3}Nb_{1.3}O_6$ based on the high-entropy strategy and bandgap engineering[23]. The

addition of perovskite-type $BiAlO_3$ into $Sr_{0.6}Ba_{0.4}Nb_2O_6$ was reported to induce remarkable incommensurate modulation and facilitate polar nanoregions (PNRs) formation, thereby optimizing energy storage properties[24]. Furthermore, a high-entropy TTB ceramic, $(Sr_{0.2}Ba_{0.2}Pb_{0.2}La_{0.2}Na_{0.2})Nb_2O_6$ was designed via equimolar multi-cation substitution, attaining a high W_{rec} of 11.0 J/cm^3 and an η of 81.9% under the electric field of 753 kV/cm, which was attributed to enhanced compositional heterogeneity and lattice distortion that reduce polarization hysteresis and improve breakdown strength[25]. Similarly, Duan *et al.* fabricated high-entropy TTB ceramics with the composition $Sr_{0.35}Ba_{0.35}Na_{0.1}Ca_{0.1}Bi_{0.1}Nb_{1.8}Ta_{0.2}O_6$. The introduction of multiple cations promotes the formation of PNRs, which effectively lowers domain-switching energy barriers and weakens interdomain coupling. This synergistic effect thereby delays polarization saturation and leads to enhanced energy-storage performance[26]. While the aforementioned studies have successfully enhanced the energy-storage performance of $Sr_xBa_{1-x}Nb_2O_6$ ceramics through various elemental doping strategies, it should not be overlooked that the sintering aids also play an important role in determining energy-storage performance.

$Sr_{0.6}Ba_{0.4}Nb_2O_6$ ceramics exhibit typical relaxor ferroelectric characteristics, with a broad phase transition temperature around 50 °C[24], providing a promising basis for achieving high energy-storage performance. Here, we propose a feasible and practical strategy to further enhance the energy-storage performance of $Sr_{0.6}Ba_{0.4}Nb_2O_6$ ceramics through the selective use of sintering aids, including MnO_2, CuO, and Li_2CO_3. The effects of these additives on microstructure, dielectric response, and energy-storage performance and related mechanisms are illustrated. The results reveal that the outstanding performance of the CuO-modified ceramics correlates with enhanced densification and a widened band gap, which collectively improve the E_b. Moreover, the significantly enhanced relaxor degree is beneficial for reducing polarization loss. This combination of enhanced E_b and reduced polarization loss ultimately leads to an improved energy storage density. This work provides a viable method for enhancing the intrinsic energy-storage performance of $Sr_{0.6}Ba_{0.4}Nb_2O_6$ (SBN)-based ceramics.

MATERIALS AND METHODS

The SBN (defined as S0) ceramic and its variants modified with sintering aids (MnO_2, CuO, and Li_2CO_3, designated as S1, S2, and S3, respectively) were synthesized using a conventional solid-state reaction method. High-purity starting materials in this work were supplied by Aladdin Reagent Co., LTD (China). Firstly, $BaCO_3$ (99%), $SrCO_3$ (99%), and Nb_2O_5 (99.9%) were weighed according to the target stoichiometry. These powders were mixed via ball milling in an alcohol medium for 12 h. The blended slurry was then dried and calcined at 1,150 °C for 2 h to form the desired crystalline phase. Next, the different sintering aids, including MnO_2 (99.9%), CuO (99.0%), and Li_2CO_3 (99.0%), were added in a proportion of 0.2 wt%. The concentration of 0.2 wt% was selected based on a previous study[27], which reported that this amount is effective for tungsten bronze-structured relaxor ceramics. The mixed powders were again milled to improve homogeneity. Following this, the fine powders were granulated and compacted to form uniform green bodies. Finally, densification was achieved by sintering the compacts at 1,250-1,350 °C for 2 h in air to yield the final ceramics.

The crystalline phase structure of the sintered pellets was characterized by X-ray diffraction (XRD, Shimadzu XRD-6100, Japan) over a 2θ range of 10°-120° at a scan rate of 2 °/min. Surface morphology was examined using a field-emission scanning electron microscope (FE-SEM, TESCAN MAIA3 LMH, Czech Republic). Raman spectroscopy was conducted on a Horiba Jobin Yvon LabRAM HR Evolution spectrometer with a 532.3 nm excitation source. For dielectric measurements, the samples were polished to a thickness of 0.8 mm and coated with silver paste on both surfaces, and then were evaluated using an Inductance-Capacitance-Resistance (LCR) meter (Agilent E4980A, USA) at an applied voltage of 1 V. For ferroelectric hysteresis loop

measurements, all specimens were polished to 0.10-0.15 mm and sputtered with Pt circular electrodes 2 mm in diameter, characterized by a ferroelectric working station (Precision Premier II, Radiant Company). Ultraviolet-visible (UV-vis) absorption spectra were obtained by a UV-vis Spectrometer (PerkinElmer Lambda 950, China). X-ray photoelectron spectroscopy (XPS, Thermo Scientific ESCALAB 250Xi, USA) was used to observe the existence of oxygen vacancies. Local crystallographic structure and selected area electron diffraction (SAED) were investigated by bright-field transmission electron microscopy (BF-TEM, JEOL JEM-F200, Japan).

RESULTS AND DISCUSSION

Energy storage performance of sintering aids-modulated SBN ceramics

To investigate the effects of various sintering aids on energy storage performance, unipolar polarization-electric field (*P-E*) hysteresis loops were measured for all samples at their respective E_b, as presented in Figure 1A. All loops exhibit similar trends under the applied electric field and consistently show low P_r, an intrinsic characteristic of SBN ceramics. Figure 1B illustrates the dependence of P_m, P_r, and ΔP on the sintering aids. The incorporation of sintering aids systematically enhances P_m while maintaining an almost constant P_r. As a result, a significant improvement in ΔP is achieved, underscoring the effectiveness of sintering aids in optimizing polarization behavior. Specifically, the measured P_m values are 21.89, 24.47, 29.38, and 24.59 μC/cm², with the S2 sample achieving the highest ΔP of 26.59 μC/cm². Consequently, the S2 sample demonstrates the optimal energy storage performance [Figure 1C], delivering a W_{rec} of 4.41 J/cm³ and an η of 93.4%. Figure 1D presents the *P-E* hysteresis loops of the S2 ceramic under varying electric fields. As the electric field strength increases, the P_m rises gradually without reaching clear saturation, indicating favorable potential for further optimization of energy storage performance. As summarized in Supplementary Table 1, the S2 ceramic exhibits superior W_{rec} and η compared to recently reported TTB-structured ceramics, highlighting its potential for high-performance energy storage applications. The underlying mechanisms responsible for the superior performance of the S2 sample will be discussed in detail in the following section.

Microstructural origin of enhancement in energy storage performance

Figure 2A visualizes a schematic of the SBN lattice structure projected along the [001] axis. In this structure, the C site remains vacant, while the A and B sites are partially occupied: only 5/6 of the A positions are filled, with the remaining 1/6 left empty[28]. Notably, due to its larger ionic radius (1.61 Å), Ba^{2+} tends to occupy the larger A2 site, whereas the smaller Sr^{2+} (1.44 Å) occupies both the A1 site and the remaining A2 positions. Raman spectroscopy was performed in the range of 150-1,000 cm^{-1}, with the spectra shown in Figure 2B. The observed features match those previously reported for TTB-type ceramics, confirming the characteristic vibrational modes of the TTB structure. The ν_5 mode near 250 cm^{-1} is assigned to O-B-O bending vibrations, and the ν_2 mode around 630 cm^{-1} is corresponding to B-O stretching vibrations[29]. No discernible changes in these modes were observed following the addition of sintering aids, suggesting that the sintering aids themselves do not alter the local structure. XRD patterns of all samples are presented in Figure 2C. They show good agreement with the standard reference (JCPDS No. 88-0785) and no detectable secondary phases, indicating that the addition of sintering aids does not induce phase separation. Rietveld refinement of the XRD data was performed, with the results presented in Supplementary Figure 1 and the detailed lattice parameters summarized in Supplementary Table 2. All samples were indexed to the pure *P4bm* space group. Notably, the introduction of sintering aids results in varying degrees of change in the lattice parameters, indicating that these additives can partially enter the crystal lattice of the matrix. To evaluate the effect of sintering aids on densification, the measured and relative density of the ceramics are summarized in Figure 2D. Ceramics modified with sintering aids exhibit relative densities exceeding 98%, higher than the 96.7% achieved for the unmodified SBN ceramic.

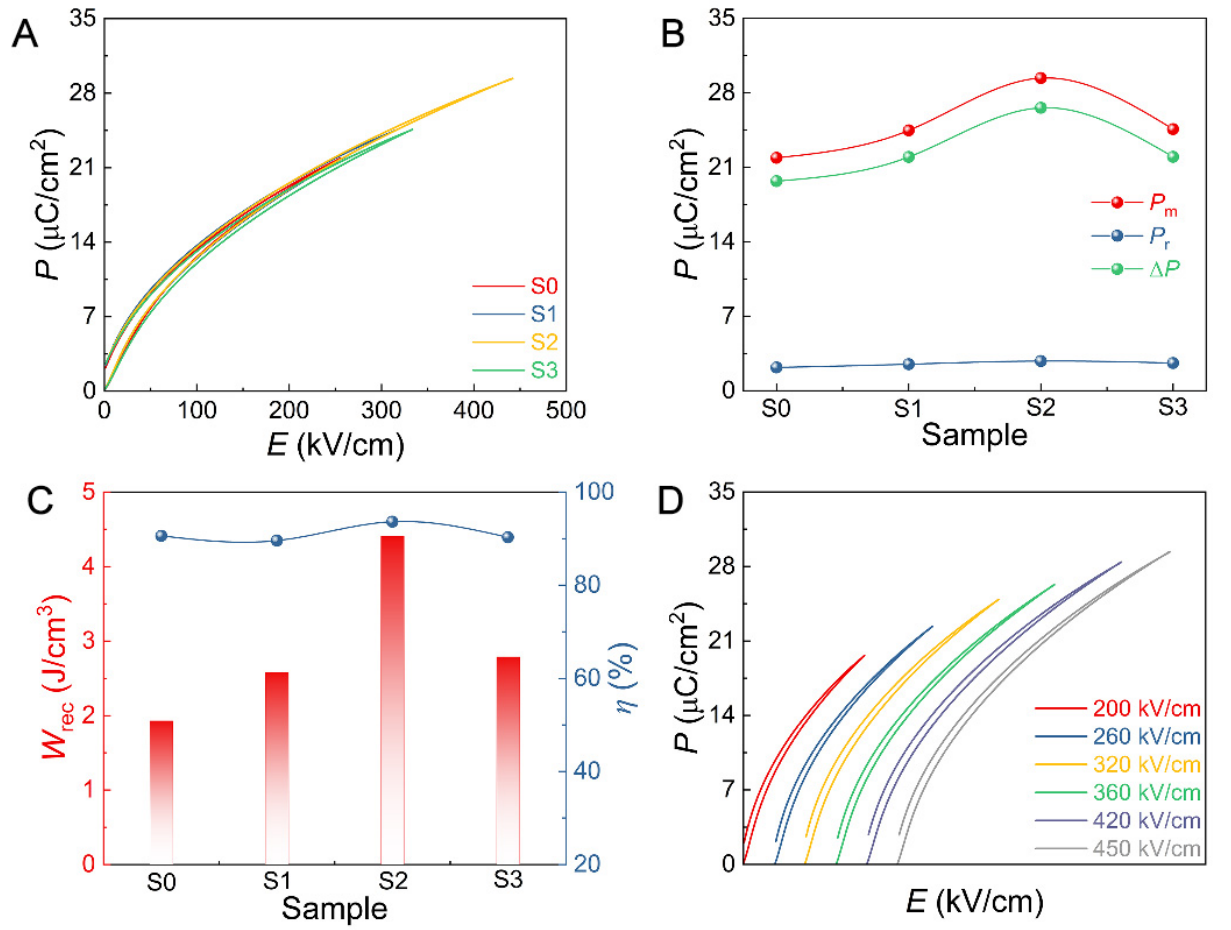

Figure 1. (A) *P-E* hysteresis loops, (B) P_m, P_r, and ΔP, (C) W_{rec} and η, and (D) Electric field-dependent *P-E* hysteresis loops for S2 ceramic. *P-E*: Polarization-electric field.

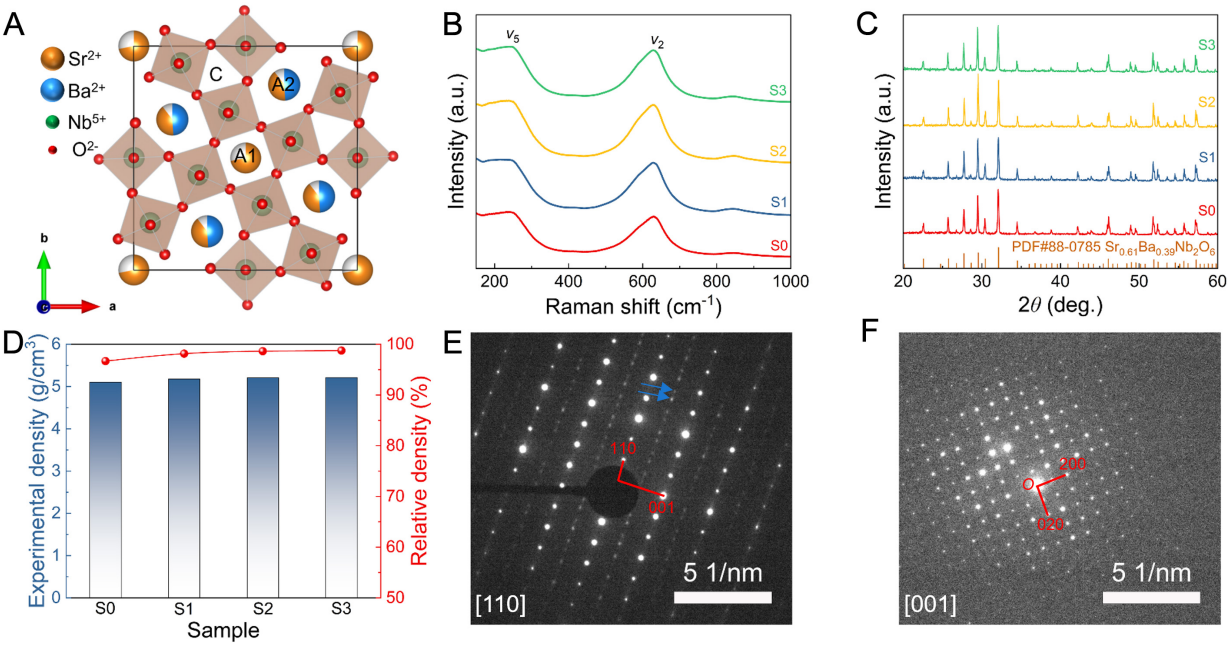

Figure 2. (A) Schematic of the SBN lattice structure projected along the [001] axis; (B) Raman spectra, (C) XRD patterns, and (D) measured actual density along with relative density of all SBN ceramics; SAED patterns of S2 ceramic projected along the (E) [110] axis and (F) [001] axis. SBN: $Sr_{0.6}Ba_{0.4}Nb_2O_6$; XRD: X-ray diffraction; SAED: selected-area electron diffraction.

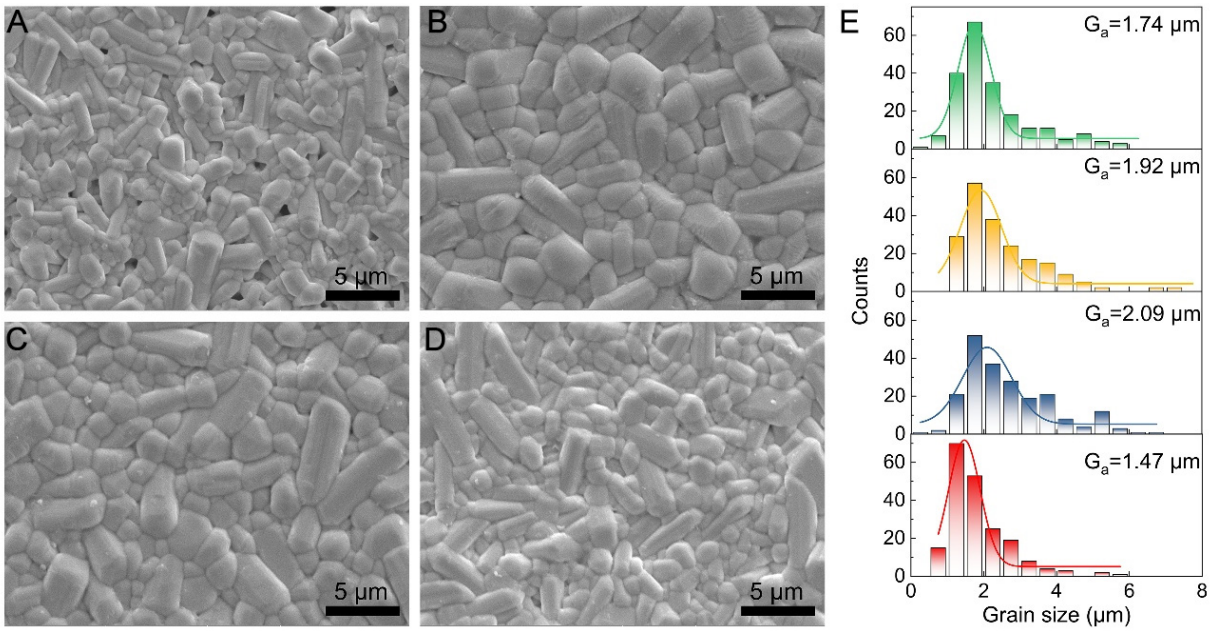

Figure 3. SEM images of (A) S0, (B) S1, (C) S2, (D) S3 samples; (E) grain size distribution of the SBN ceramics. SBN: $Sr_{0.6}Ba_{0.4}Nb_2O_6$; SEM: scanning electron microscope.

The phase structures of the S2 ceramic were further characterized using transmission electron microscopy (TEM), as shown in Figure 2E-F. Along the [110] and [001] zone axes, the basic SAED patterns can be indexed to a standard TTB structure. Notably, superlattice spots are observed along the [110] zone axis, which can be attributed to A-site cation distortion, consistent with previous reports[30]. Specifically, the A-site cation distortion, as evidenced by these superlattice spots, introduces local random fields that disrupt the long-range ferroelectric order. This disruption promotes the formation of PNRs, which are widely recognized as the hallmark of relaxor ferroelectrics.

Figure 3A-D present the surface SEM images of all SBN ceramics, with their corresponding grain size distributions displayed in Figure 3E. All compositions exhibit a microstructure consisting of a mixture of equiaxed and pillar-type grains. Notably, the unmodified S0 ceramic exhibits a few residual pores, whereas the addition of sintering aids reduced porosity and resulted in a marked improvement in densification. This enhanced densification directly contributes to superior breakdown resistance. On one hand, fewer pores reduce local electric field concentration, delaying breakdown initiation. On the other hand, a more compact microstructure effectively hinders the propagation of breakdown pathways. Based on Gaussian fitting, the average grain sizes are determined to be 1.47, 2.09, 1.92, and 1.74 μm, indicating that the sintering aids promote grain growth to a certain degree. This enhanced densification and grain coarsening can be attributed to the effects of the MnO_2/CuO/Li_2CO_3 sintering additives. During the sintering process, a liquid phase forms, facilitating mass transport and thereby promoting grain growth and densification[27,31,32]. As illustrated in Supplementary Figures 2-5, the homogeneous distribution of Mn and Cu with no observable segregation confirms that these ions have been incorporated uniformly into the SBN lattice. The improved densification and uniform elemental distribution are favorable for the optimization of the electrical properties.

In this work, the introduction of sintering aids (MnO_2, CuO, and Li_2CO_3) enables the incorporation of Mn^{4+}, Li^+, and Cu^{2+} ions into B sites of the lattice, where they substitute for Nb^{5+}. This aliovalent substitution necessitates charge compensation, leading to the formation of oxygen vacancies (V_O'')[33]. These oxygen

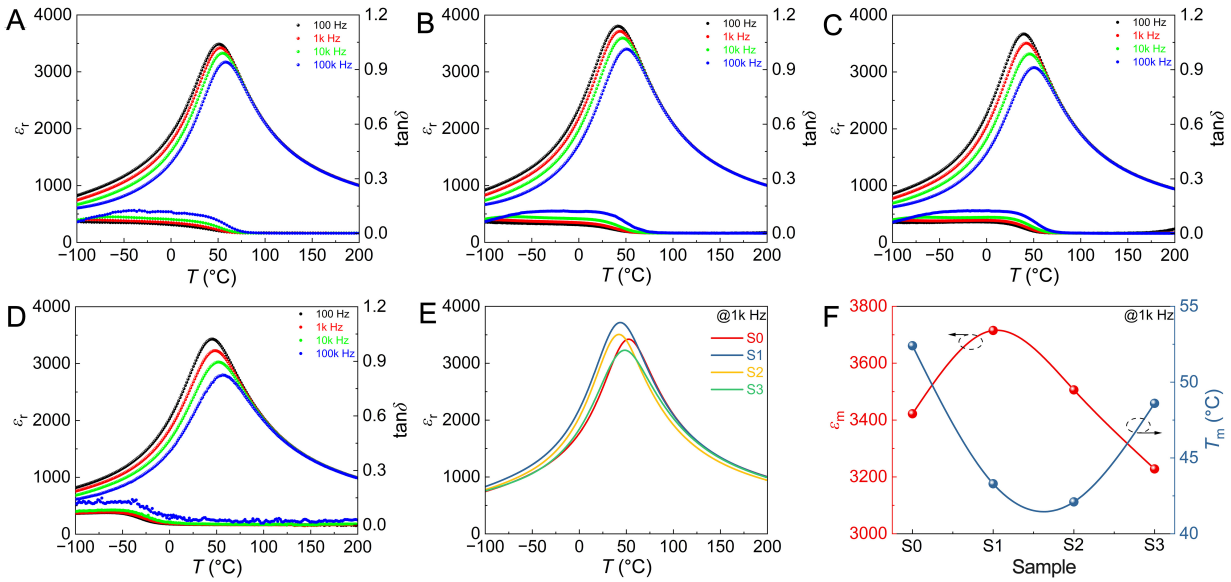

Figure 4. Temperature-dependent dielectric properties of (A) S0, (B) S1, (C) S2, (D) S3 samples; (E) Comparison of temperature-dependent ε_r for all samples measured at 1 kHz; (F) ε_m and corresponding T_m for all samples at 1 kHz.

vacancies tend to form defect dipoles with lattice defects, such as Mn_{Nb}'. Subsequently, these dipoles locally aggregate and couple to form defect clusters[34]. As a result, the concentration of mobile charge carriers decreases, enhancing the insulation properties of the ceramics. To further investigate the existence of oxygen vacancies, XPS analysis was performed, and the results are displayed in Supplementary Figure 6. The O 1s spectra of all ceramics could be deconvoluted into three distinct peaks via Avantage software, corresponding to lattice oxygen (O_L), oxygen vacancies (O_V), and adsorbed oxygen (O_H)[35].

Taken together, these structural analyses demonstrate that the incorporation of sintering aids effectively promotes densification while preserving the single-phase TTB structure of SBN. These microstructural advantages underpin the enhanced energy storage performance observed in the corresponding samples.

Electrical properties origin of enhancement in energy storage performance

To explore the origin of the electrical properties and the enhancement in energy storage performance, temperature-dependent dielectric permittivity (ε_r) and dielectric loss (tanδ) for all SBN ceramics are depicted in Figure 4A-D. All samples exhibit frequency dispersion with a broad phase transition temperature (T_m), indicative of typical relaxor behavior. Figure 4E compares the temperature-dependent ε_r across compositions, while the maximum permittivity (ε_m) and the corresponding T_m measured at 1 kHz are summarized in Figure 4F. The incorporation of sintering additives moderately influences the dielectric properties. Notably, the ε_r values of S1, S2, and S3 at room temperature are higher than those of S0. This increase in ε_r, accompanied by consistently low tanδ, is attributed to improved domain wall mobility and facilitated polarization rotation. Moreover, the addition of sintering aids leads to a decrease in T_m, which can be explained by the enhanced random fields introduced by the additives.

As a typical relaxor ferroelectric, SBN exhibits characteristic relaxor dispersion. Figure 5A presents the relaxation temperature span ΔT_{relax} (defined as T_m at 100 kHz minus T_m at 100 Hz) for each sample. ΔT_{relax} progressively increases from 7.4 °C for S0 to 9.1 °C for S1, 11.6 °C for S2, and finally to 12.4 °C for S3. Furthermore, a modified Curie-Weiss law is used to evaluate the relaxor degree[36,37]:

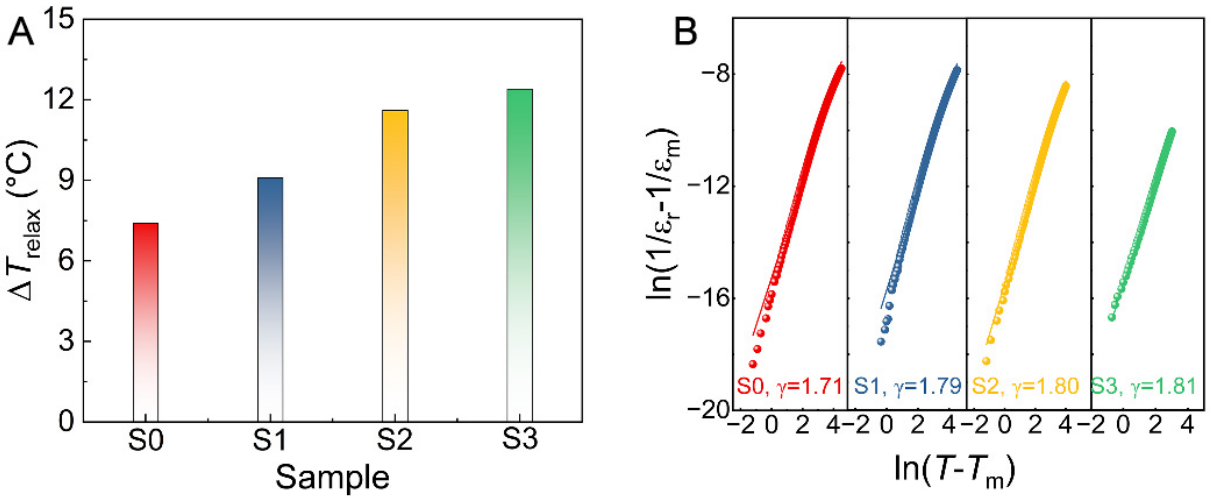

Figure 5. (A) Comparison of ΔT_{relax} for all samples; (B) Plot of $\ln(1/\varepsilon\text{-}1/\varepsilon_m)$ versus $\ln(T\text{-}T_m)$ at 1 kHz.

$$\frac{1}{\varepsilon} - \frac{1}{\varepsilon_m} = \frac{(T - T_m)^\gamma}{C} \tag{4}$$

A value of $\gamma = 1$ corresponds to normal ferroelectric behavior, whereas $\gamma = 2$ indicates ideal relaxor characteristics. The fitted γ values for S0-S3 are 1.71, 1.79, 1.80, and 1.81, respectively [Figure 5B]. These results provide powerful evidence that the addition of sintering additives effectively enhance the relaxor nature of the SBN ceramics, which originates from the formation of random fields and compositional disorder within the lattice.

To evaluate the influence of the additive on the band gap, UV-vis absorption spectra [Figure 6A] were measured and analyzed using the Tauc plot method, expressed as[38,39]:

$$(\alpha h\nu)^{\frac{1}{n}} = A\left(h\nu - E_g\right) \tag{5}$$

where α, h, ν, E_g denote the absorption coefficient, Planck's constant, frequency, and band gap. A is a constant, and n is an index taken as 1/2 for dielectric ceramics. The calculated E_g values for all samples are 3.31, 3.28, 3.29, and 3.26 eV [Figure 6B], indicating good insulating properties. While the band gap width is generally considered to influence the intrinsic breakdown strength of dielectric materials, the variation in E_g among the samples is relatively small and cannot solely account for the significant differences observed in E_b. The substantial enhancement of E_b following the introduction of sintering aids is therefore primarily attributed to enhanced densification. The breakdown behavior was further assessed using Weibull statistics. Figure 6C displays the Weibull distributions fitted with the equation[40,41]:

$$P\left(E_i\right) = 1 - \exp\left[-\left(\frac{E_i}{E_b}\right)^\beta\right] \tag{6}$$

where E is the applied electric field, $P(E)$ presents the cumulative probability at E, E_b is the characteristic breakdown strength [$P(E) = 63.2\%$], and β is the shape parameter that reflects data reliability (higher indicates better reliability). The fitted E_b values are 255.9, 342.6, 442.3, and 343.7 kV/cm, as shown in Figure 6D. The highest E_b achieved in S2 is consistent with its superior energy storage performance shown in Figure 1C.

In conclusion, the addition of sintering aids plays a crucial dual role in optimizing the ceramic's energy storage performance. Firstly, it enhances densification, which effectively suppresses premature failure under

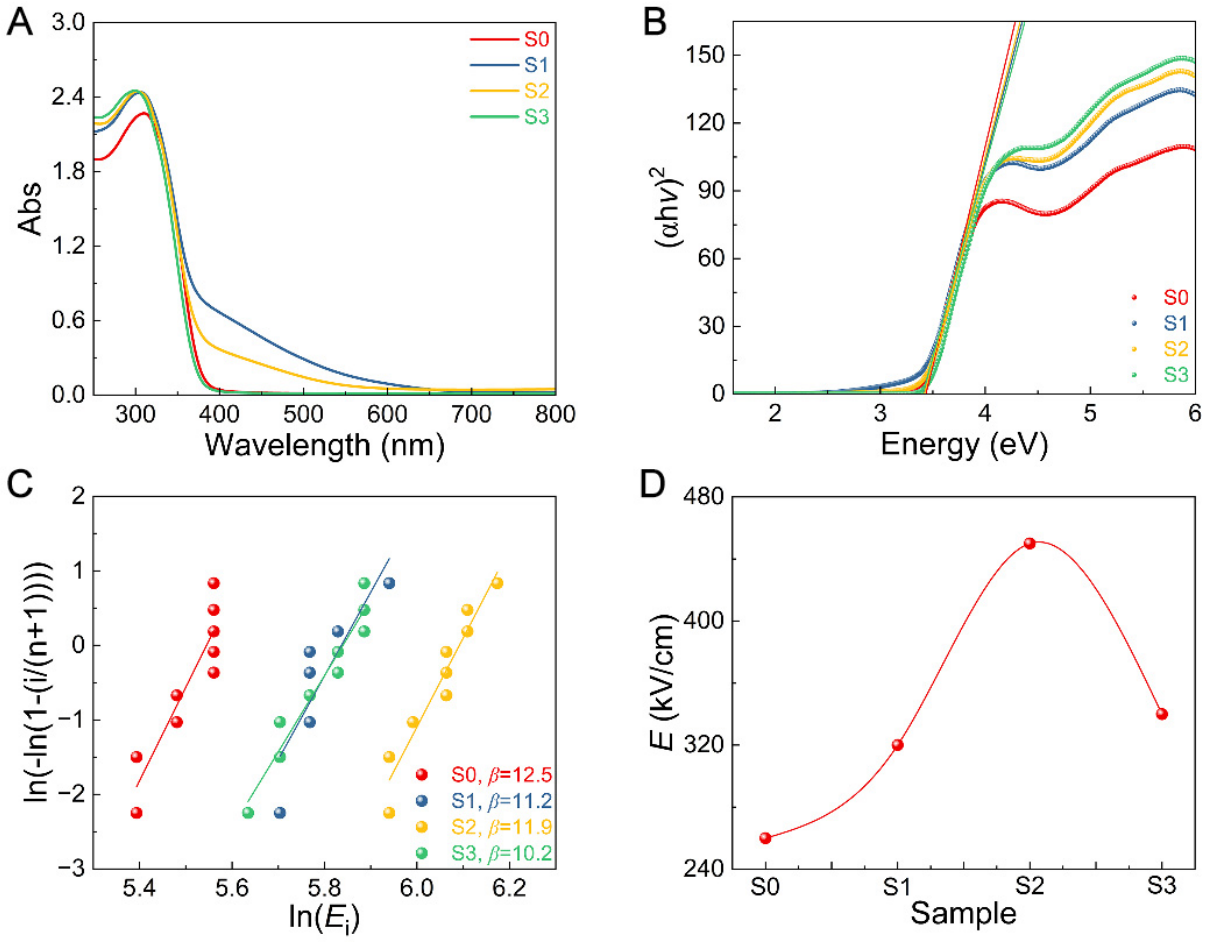

Figure 6. (A) UV-vis absorption spectra, (B) Tauc plots, (C) Weibull distributions of the applied electric fields, and (D) E_b values for all SBN ceramics. UV-vis: Ultraviolet-visible; SBN: $Sr_{0.6}Ba_{0.4}Nb_2O_6$.

high electric fields, thereby improving the breakdown strength. Secondly, it strengthens the relaxor characteristics, which minimizes hysteresis losses during charge-discharge cycles. The combination of a higher breakdown strength and lower polarization loss ultimately yields a markedly improved overall energy storage performance.

Thermal and frequency stability

Furthermore, the thermal and frequency stability of the S2 ceramic was evaluated under an applied electric field of 320 kV/cm, as shown in Figure 7. Within the temperature range of 25-125 °C, the W_{rec} consistently exceeds 2.75 J/cm^3, with variation below 10%, while the η remains above 91%. Notably, both W_{rec} and η also exhibit outstanding frequency stability, with variations of less than 2% across the measured frequency range. The excellent thermal stability can be attributed to the relaxor behavior and uniform microstructure promoted by the CuO sintering aid, which suppresses polarization degradation and loss increase at elevated temperatures. Overall, the CuO-modified SBN ceramics show remarkable stability in both temperature and frequency, underscoring their great potential for use in advanced pulse power devices.

CONCLUSIONS

In summary, different sintering aids (MnO_2, CuO, and Li_2CO_3)-modified tetragonal tungsten bronze SBN ceramics were prepared via the traditional solid-state sintering process. Comprehensive structural characterizations including XRD, SEM, Raman spectra, and TEM demonstrate that the incorporation of

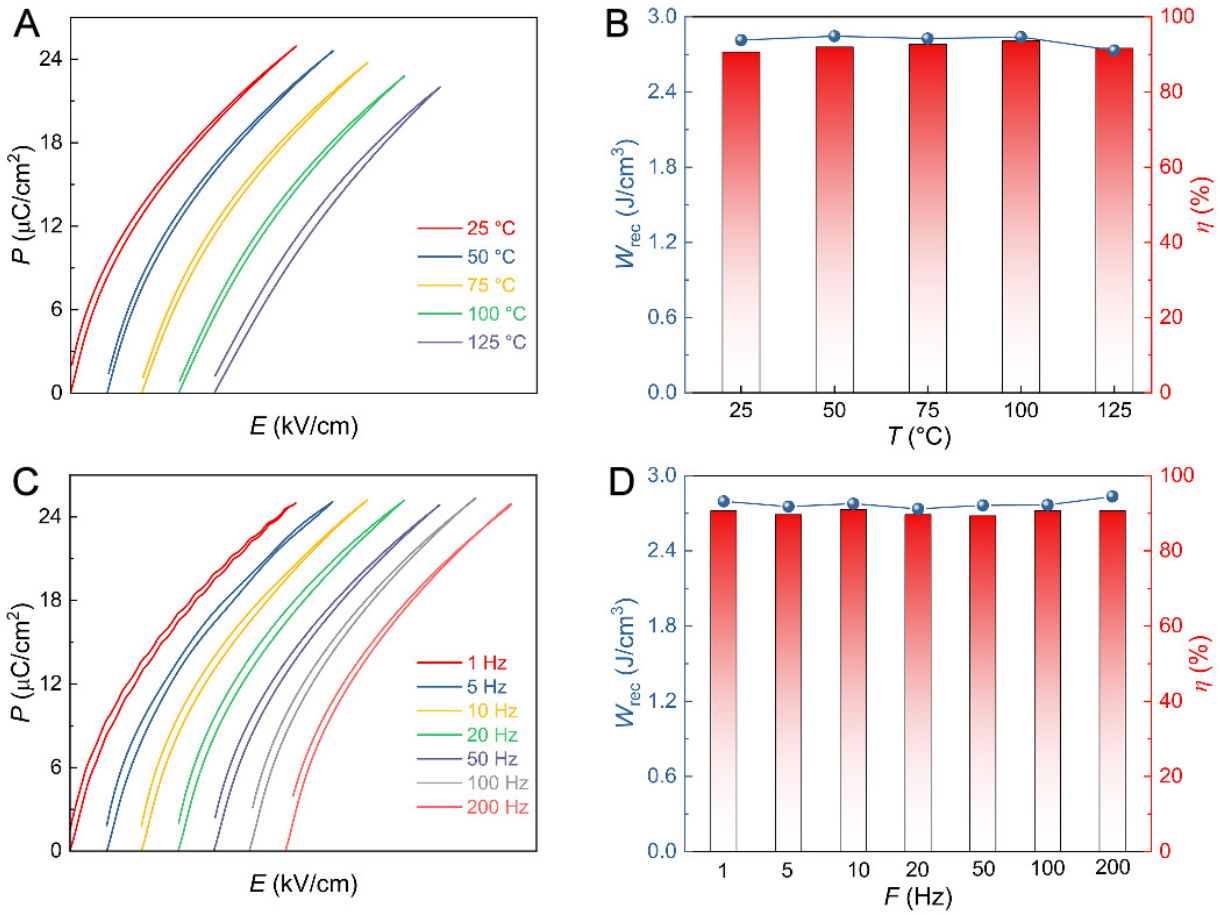

Figure 7. (A) *P-E* hysteresis loops; (B) W_{rec} and η for S2 sample within the temperature range of 25-125 °C under 320 kV/cm; (C) *P-E* hysteresis loops; (D) W_{rec} and η for S2 sample within the frequency range of 1-200 Hz under 320 kV/cm. *P-E*: Polarization-electric field.

sintering additives effectively promotes densification and strengthens relaxor character. Finally, we obtained a high W_{rec} of 4.41 J/cm³ and an η of 93.4% in CuO-modified SBN ceramics. The ceramic also exhibits excellent thermal and frequency stability, maintaining a W_{rec} above 2.75 J/cm³ with less than 10% variation under varying conditions. These results clarify the role of sintering aids in enhancing energy storage performance and provide guidance in tailoring SBN energy-storage ceramics.

DECLARATIONS

Acknowledgments

We would like to thank Chao Feng at the Instrument Analysis Center of Xi'an Jiaotong University for the assistance with UV-vis absorption spectra characterization. Also, we thank the Public Research Platform at the State Key Laboratory of Electrical Insulation and Power Equipment.

Authors' contributions

Investigation, conceptualization, methodology, validation, writing - original draft, writing - review & editing, funding acquisition: Kang, R.
Investigation, formal analysis, data curation: Hu, H.
Formal analysis, methodology: Xu, J.
Validation, funding acquisition: Yang, B.
Formal analysis, funding acquisition: Zhao, Y.
Validation, data curation, writing - review & editing, funding acquisition: Gao, Y.
Supervision: Shao, J.
Resources, writing - review & editing, supervision, funding acquisition: Lou, X.

Availability of data and materials

The data that support the findings of this study are available from the corresponding author upon reasonable request.

AI and AI-assisted tools statement

During the preparation of this manuscript, the AI tool ChatGPT (version 5.5, released 2026-04-23) was used solely for language editing. The tool did not influence the study design, data collection, analysis, interpretation, or the scientific content of the work. All authors take full responsibility for the accuracy, integrity, and final content of the manuscript.

Financial support and sponsorship

This work was supported by the National Natural Science Foundation of China (Nos. 52572141, 52572262, 52502153 and 52302155), Natural Science Basic Research Program of Shaanxi Province (2025JC-YBQN-579), Postdoctoral Fellowship Program of CPSF (GZC20250353), China Postdoctoral Science Foundation (2024M762584), Science and Technology Plan Project of Xi'an Beilin District of Shaanxi Province (GX2432) and Fundamental Research Funds for the Central Universities (Nos. xzy012025104 and xzd012025006).

Conflicts of interest

All authors declared that there are no conflicts of interest.

Ethical approval and consent to participate

Not applicable.

Consent for publication

Not applicable.

Copyright

© The Author(s) 2026.

Supplementary Materials

Supplementary Materials

REFERENCES

1. Jayakrishnan, A.; Silva, J.; Kamakshi, K.; et al. Are lead-free relaxor ferroelectric materials the most promising candidates for energy storage capacitors? *Prog. Mater. Sci.* **2023**, *132*, 101046. DOI
2. Zhang, L.; Jing, R.; Zhang, S.; Jin, L. Multiscale microstructure design for high-performance dielectric energy storage materials. *Microstructures* **2026**, *6*, 2026002. DOI
3. Cao, W.; Wu, Y.; Yang, X.; et al. Breaking polarization-breakdown strength paradox for ultrahigh energy storage density in NBT-based ceramics. *Nat. Commun.* **2025**, *16*, 6228. DOI PubMed PMC
4. Yan, F.; Wang, S.; Qian, J.; et al. Tape-casting lead-free dielectrics permit superior capacitive energy storage performance. *Adv. Energy. Mater.* **2025**, *15*, 2403535. DOI
5. Dan, Y.; Tang, L.; Ning, W.; Hu, C.; Liu, L.; Fang, L. Enhancing energy storage performance in tungsten bronze ceramics utilizing site engineering. *Microstructures* **2025**, *5*, 2025050. DOI
6. Wang, G.; Lu, Z.; Li, Y.; et al. Electroceramics for high-energy density capacitors: current status and future perspectives. *Chem. Rev.* **2021**, *121*, 6124-72. DOI PubMed PMC
7. Luo, B.; Wang, X.; Tian, E.; Song, H.; Wang, H.; Li, L. Enhanced energy-storage density and high efficiency of lead-free $CaTiO_3$-$BiScO_3$ linear dielectric ceramics. *ACS. Appl. Mater. Interfaces.* **2017**, *9*, 19963-72. DOI
8. Guo, X.; Pu, Y.; Wang, W.; et al. Ultrahigh energy storage performance and fast charge-discharge capability in Dy- modified $SrTiO_3$ linear ceramics with high optical transmissivity by defect and interface engineering. *Ceram. Int.* **2020**, *46*, 21719-27. DOI
9. Wang, W.; Pu, Y.; Guo, X.; Shi, R.; Yang, M.; Li, J. Combining high energy efficiency and fast charge-discharge capability in calcium strontium titanate-based linear dielectric ceramic for energy-storage. *Ceram. Int.* **2020**, *46*, 11484-91. DOI
10. Yang, Z.; Du, H.; Jin, L.; Poelman, D. High-performance lead-free bulk ceramics for electrical energy storage applications: design strategies and challenges. *J. Mater. Chem. A.* **2021**, *9*, 18026-85. DOI

11. Yang, Y.; Li, Y.; Song, Y.; et al. Lead-free trirelaxor ferroelectrics: high energy storage capacity in the paraelectric state and broad operating temperature range. *Adv. Mater.* **2026**, *38*, e09323. DOI
12. Cao, W.; Li, T.; Li, K.; et al. Unleashed remarkable energy storage performance in $Bi_{0.5}K_{0.5}TiO_3$-based relaxor ferroelectrics by local structural fluctuation. *Angew. Chem. Int. Ed.* **2025**, *64*, e202416291. DOI
13. Zhao, W.; Xu, D.; Li, D.; et al. Broad-high operating temperature range and enhanced energy storage performances in lead-free ferroelectrics. *Nat. Commun.* **2023**, *14*, 5725. DOI PubMed PMC
14. Li, J.; Shen, Z.; Chen, X.; et al. Grain-orientation-engineered multilayer ceramic capacitors for energy storage applications. *Nat. Mater.* **2020**, *19*, 999-1005. DOI
15. Chen, L.; Hu, T.; Shi, X.; et al. Near-zero energy consumption capacitors by controlling inhomogeneous polarization configuration. *Adv. Mater.* **2024**, *36*, e2313285. DOI
16. Chen, L.; Wang, N.; Zhang, Z.; et al. Local diverse polarization optimized comprehensive energy-storage performance in lead-free superparaelectrics. *Adv. Mater.* **2022**, *34*, e2205787. DOI
17. Li, D.; Zhou, D.; Wang, D.; Zhao, W.; Guo, Y.; Shi, Z. Improved energy storage properties achieved in (K, Na)NbO_3-based relaxor ferroelectric ceramics via a combinatorial optimization strategy. *Adv. Funct. Mater.* **2022**, *32*, 2111776. DOI
18. Zhang, M.; Yang, H.; Lin, Y.; Yuan, Q.; Du, H. Significant increase in comprehensive energy storage performance of potassium sodium niobate-based ceramics via synergistic optimization strategy. *Energy. Storage. Mater.* **2022**, *45*, 861-8. DOI
19. Cao, L.; Yuan, Y.; Meng, X.; Li, E.; Tang, B. Ferroelectric-relaxor crossover and energy storage properties in Sr(2)NaNb(5)O(15)-based tungsten bronze ceramics. *ACS. Appl. Mater. Interfaces.* **2022**, *14*, 9318-29. DOI
20. Xu, S.; Tian, M.; Yu, P.; et al. A novel multifunctional SANNS-based tungsten bronze ceramic with excellent energy storage and photoluminescence capabilities. *J. Alloy. Compd.* **2025**, *1036*, 182069. DOI
21. Duan, J.; Wei, K.; Qi, H.; et al. $Sr_{0.6}Ba_{0.4}NbO_6$ superparaelectrics with simple composition and high-efficiency capacitive energy storage. *Chem. Eng. J.* **2025**, *516*, 164009. DOI
22. Alhazmi, M.; Ali, A. I.; Choi, D.; et al. Superior energy storage properties of $(Ba_{0.4}Ca_{0.3}Sr_{0.3})Nb_2O_6$ bronze structure based Nd^{3+}/Sb^{5+} ions via entropy and interfacial polarization strategies. *J. Alloy. Compd.* **2025**, *1041*, 183771. DOI
23. Tang, L.; Ning, W.; Wu, S.; et al. Energy storage performance of high-entropy SBN-based tungsten bronze-structure ceramic. *J. Alloy. Compd.* **2025**, *1015*, 178902. DOI
24. Feng, J.; Zheng, P.; Wang, T.; et al. Realizing high energy storage performances in $Sr_{0.6}Ba_{0.4}Nb_2O_6$-based tungsten bronze-perovskite heterogeneous solid solution ceramics. *Mater. Today. Energy.* **2025**, *54*, 102082. DOI
25. Peng, H.; Wu, T.; Liu, Z.; et al. High-entropy relaxor ferroelectric ceramics for ultrahigh energy storage. *Nat. Commun.* **2024**, *15*, 5232. DOI PubMed PMC
26. Duan, J.; Wei, K.; Du, Q.; Ma, L.; Qi, H.; Li, H. High-entropy tungsten bronze ceramics for large capacitive energy storage with near-zero losses. *Adv. Funct. Mater.* **2024**, *34*, 2409446. DOI
27. Zhang, X.; Zheng, P.; Li, L.; et al. High energy storage performance in tungsten bronze-based relaxor ceramic via doping with CuO. *Scr. Mater.* **2022**, *211*, 114514. DOI
28. Li, C.; Zhang, Y.; Liu, J.; Graetsch, H. A. Long-range and local structure of $Sr_xBa_{1-x}Nb_2O_6$ (x= 0.33 and 0.67) across the ferroelectric-relaxor transition. *Chem. Mater.* **2020**, *32*, 1844-53. DOI
29. Peng, H.; Liu, Z.; Fu, Z.; et al. Superior energy density achieved in unfilled tungsten bronze ferroelectrics via multiscale regulation strategy. *Adv. Sci.* **2023**, *10*, e2300227. DOI PubMed PMC
30. Kang, R.; Wang, Z.; Gao, Y.; Yuan, W.; Shao, J.; Lou, X. High energy storage in tetragonal tungsten bronze ceramics engineered via superparaelectric state. *Appl. Phys. Lett.* **2026**, *128*, 152903. DOI
31. Zhong, X.; Shui, A.; Fang, Y.; Yu, H. Improved relaxor behavior and insulation in $BaTiO_3$-based ceramics for high-performance energy storage via trace MnO_2 doping. *Ceram. Int.* **2025**, *51*, 66103-12. DOI
32. Zhao, L.; Zhang, B.; Zhou, P.; Zhao, X.; Zhu, L.; Damjanovic, D. Phase structure and property evaluation of (Ba,Ca)(Ti,Sn)O_3 sintered with Li_2CO_3 addition at low temperature. *J. Am. Ceram. Soc.* **2014**, *97*, 2164-9. DOI
33. Ren, X. Large electric-field-induced strain in ferroelectric crystals by point-defect-mediated reversible domain switching. *Nat. Mater.* **2004**, *3*, 91-4. DOI PubMed
34. Hu, W.; Liu, Y.; Withers, R. L.; et al. Electron-pinned defect-dipoles for high-performance colossal permittivity materials. *Nat. Mater.* **2013**, *12*, 821-6. DOI
35. Dong, Q.; Zhang, Y.; Pan, Y.; et al. Defect-engineered core-shell structured $NaNbO_3$-based energy storage ceramics. *J. Materiomics.* **2026**, *12*, 101097. DOI

36. Zhang, M.; Lan, S.; Yang, B. B.; et al. Ultrahigh energy storage in high-entropy ceramic capacitors with polymorphic relaxor phase. *Science* **2024**, *384*, 185-9. DOI
37. Dan, Y.; Tang, L.; Ning, W.; et al. Achieving enhanced energy storage performance and ultra-fast discharge time in tungsten-bronze ceramic. *J. Adv. Ceram.* **2024**, *13*, 1349-58. DOI
38. Liu, P.; Ren, X.; Qian, J.; et al. Polymorphic superparaelectric engineering boosting energy storage capacity in $BaTiO_3$-based ceramics. *Adv. Sci.* **2026**, , e24252. DOI
39. Ye, H.; Yang, F.; Pan, Z.; et al. Significantly improvement of comprehensive energy storage performances with lead-free relaxor ferroelectric ceramics for high-temperature capacitors applications. *Acta. Mater.* **2021**, *203*, 116484. DOI
40. Wang, S.; Qian, J.; Ge, G.; et al. Embedding plate-like pyrochlore in perovskite phase to enhance energy storage performance of BNT-based ceramic capacitors. *Adv. Energy. Mater.* **2025**, *15*, 2403926. DOI
41. Li, D.; Liu, Z.; Zhao, W.; et al. Global-optimized energy storage performance in multilayer ferroelectric ceramic capacitors. *Nat. Commun.* **2025**, *16*, 188. DOI PubMed PMC

Disclaimer/Publisher's Note: All statements, opinions, and data contained in this publication are solely those of the individual author(s) and contributor(s) and do not necessarily reflect those of OAE and/or the editor(s). OAE and/or the editor(s) disclaim any responsibility for harm to persons or property resulting from the use of any ideas, methods, instructions, or products mentioned in the content.

© The Author(s) 2026. Open Access This article is licensed under a Creative Commons Attribution 4.0 International License (https://creativecommons.org/licenses/by/4.0/), which permits unrestricted use, sharing, adaptation, distribution and reproduction in any medium or format, for any purpose, even commercially, as long as you give appropriate credit to the original author(s) and the source, provide a link to the Creative Commons license, and indicate if changes were made.